International Research Journal of Engineering and Technology (IRJET) e-ISSN: 2395-0056
Volume: 09 Issue: 02 | Feb 2022 www.irjet.net p-ISSN: 2395-0072

PSO Fractional-Order PID Controller Design for DC Component Suppression of Grid-Connected Converters

Hassen Ahmed Y.[1], Kedir Abdurezak N.[2], Ali Ebrahim A.[3] Kassie Samrawit D.[2]

[1]*Graduate Student, School of Astronautics, Beihang University, Beijing, China*
[2]*Undergraduate Student, School of Mechanical and Electrical Engineering, UESTC, Chengdu, China*
[3]*Graduated, School of Information and Communication Engineering, UESTC, Chengdu, China*

Abstract - *Recently, due to widely distributed and abundant natural resources, solar and wind energy has been paid more attention for renewable energy. However, DC current injection into the grid remains a significant issue for a transformerless grid-connected converter. Injection of DC components into the grid, if excessive, can lead to problems such as accelerating the corrosion of underground network cables and pipelines, and etc. In order to overcome the above issues, in this paper, a new control strategy is proposed to suppress DC current injection for three-phase transformerless grid-connected PV inverters. It is based on accurately extracting the DC component from grid current output combined with a swarm particle optimization algorithm to adjust parameters of the DC suppression loop fractional Order PID controller. The performance of the proposed method is evaluated and compared with the pre-existing methods. The simulation and experimental results clearly show the proposed method can suppress dc components within 0.1% of rated current.*

Key Words: DC current suppression, Grid-connected converters, particle swarm optimization, Fractional order controller, PID controller.

1.INTRODUCTION

Due to widely distributed, non-polluting and abundant natural resources, solar and wind energy has been paid more and more attention in recent years. In order to utilize this renewable energy resource, Grid-Connected Inverters are the key facilities of the system. Even though the applications of electronic power inverters in grid-connected systems are obvious, there are several issues that still exist to enhance the efficiency and reliability of such systems. In particular, DC current injection into the grid remains a significant concern for a grid-connected inverter. Ideally, the output current of the inverter will be purely alternating current (AC). However, in practice, due to various reasons, unless special measures are taken, it will contain a small amount of DC components. There are several reasons to generate dc current components such as zero-drift and scaling errors of current and voltage sensors, asymmetries in the turn-on and turn-off characteristics of semiconductor switches, turn-on/off delays on the device, gate drive circuits delay, small DC offsets errors in PWM signals, and digital controller quantization errors, etc. Injection of DC component into the grid, if excessive, can lead to problems such as 1) accelerating corrosion of underground network cables and pipelines, and etc. Moreover, it causes extra loss on the loads connected to the grid. As a result, strict national and international guidelines and standards are normally in place to limit the dc current injection into the grid. For example, according to the IEEE 929-2000 standard in the USA, the maximum dc current permitted for transformerless inverter should not exceed 0.5% of the rated current [4].

One of the simplest methods to suppress DC injection is to include a line transformer between the power converter and the grid [1-4]. recently, a transformer-less grid-connected converter draws great interest, which has merits of higher efficiency, lower cost, smaller size, and overall reduced mass [2]. However, as stated earlier, Direct Current (DC) injection is still a serious issue in Transformer-less grid-connected inverters, which degrade power quality. In order to minimize DC current injection into the grid for transformer-less grid-connected inverters, several control techniques have been proposed in the literature [5-19]. One type of methods is blocking dc current with a physical capacitor [5-7].

The second type of methods is using the dc offset voltage detection and feedback control to prevent the dc current injection to the grid [8-9]. This method detects the dc offset voltage at the inverter output, and the dc component in the grid current is eliminated by feeding back the dc offset voltage to the inner loop current controller. A detecting method of dc offset voltage introduced by Sharma [8]

The third type of methods is using the dc current detection and feedback control to prevent the dc current injection to the grid [12-20]. Have the advantage of direct controlling dc current. However, its effectiveness is limited by the accuracy of the sensor to detect DC current. In [19], a neural network-based adaptive BP-PID compensation technique is proposed. However, due to the complexity of the BP neural network algorithm, it requires extensive computation time and large data storage. As mainstream literature continues to show, dc component suppression is a challenging problem in grid-connected inverter applications only by using a conventional controller. For this reason, this research combines fractional calculus with conventional PID controller to overcome shortcomings of traditional PID controller. Compared with the classical PID controller, the Fractional order PID controller has two additional parameters: integral order and differential order, which makes the setting range of the control parameters larger. As a result, a better robust control effect can be obtained. First, the dc current is extracted from the grid current waveform utilizing a Second-Order Generalized Integrator (SOGI), and a FOPID controller is

designed to mitigate dc current injection. PSO algorithm is utilized for adjusting the five parameters of FOPID controllers. The main contributions of this paper are summarized as follows.

1), a fractional order PID controller is developed with the purpose to mitigate dc component injection into the grid.

2)A particle swarm optimization algorithm is utilized to perform the optimal design for the proposed Fractional order PID (FOPID) controller

3)A second-order generalized integrator (SOGI) based dc component estimation is proposed, which does not introduce additional time delay as it doesn't require multiple time integration compared with pre-existed software-based dc extraction methods.

This paper is organized as follows. In section 2, modelling of a three-phase LCL type grid-connected inverter is demonstrated. In section 3, the proposed dc component suppression control strategy is introduced. The fractional calculus and the design of the proposed Particle Swarm Optimization (PSO-FOPID) controller is introduced in section 4 and 5, respectively. The simulation and experimental results are presented in section 6.

2. MATHEMATICAL MODEL OF LCL-GCC

A three-phase transformerless grid-connected inverter is studied in this paper, which is shown in Fig. 1. As depicted in the figure, an LCL filter is used to interface between the inverter and the grid. Where, v_{ga}, v_{gb} and v_{gc} are the three-phase grid voltages, L_1 is the inverter side inductor, L_2 is the grid side inductor, i_{1a},i_{1b},i_{1c} are three-phase inverter current, i_{ga},i_{gb},i_{gc} are respective three-phase grid current C is filter capacitor, v_{ca},v_{cb},v_{cc} are respective three-phase capacitor voltage and V_d, represents the voltage of the dc source.

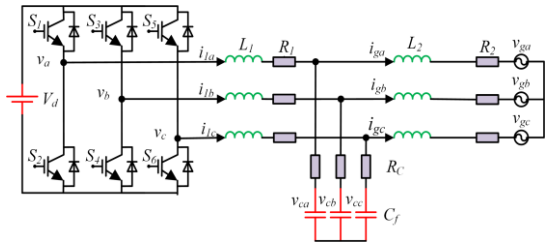

Fig-1: Original scheme diagram of three-phase PV grid-connected inverter without the proposed method

According to the KCL and KVL laws, the mathematical model of a three-phase inverter can be obtained as (1).

$$\begin{cases} L_1 \frac{di_1}{dt} = u_i - i_1 R_1 - v_c \\ L_2 \frac{di_g}{dt} = v_c - i_g R_2 - v_g \\ C \frac{dv_c}{dt} = i_1 - i_g \end{cases} \quad (1)$$

3. THE PROPOSED PSO-FPID CONTROL STRATEGY

3.1 DC Component Extraction

Compared to the AC component, the DC component in the grid current is very small. Thus, the accuracy of the DC component extraction determines the suppression effect. As stated in IEEE Standard 1547-2000, the dc component needs to be minimized within 0.5% of the rated output current [4]. In [19], the author proposed a real-time software-based DC injection detection method, which is called the sliding window double integral method (SWDIM). Similarly, based on this idea, in [20], Jiang and Yuan proposed a method called Moving Average Filter (MAF) to detect the dc component based on the multiple integration methods. Compared to low-pass filter (hardware-based), software-based methods have much higher accuracy in filtering and faster dynamic response. However, these methods are hard to match between the integration number and the dynamic response. Moreover, they will introduce additional time delay. To overcome the above issues and meet IEEE Standard 1547-2000 on dc current injection requirement, a second-order generalized integrator (SOGI) dc component estimation approach, which doesn't require multiple time integration, is proposed. A general SOGI estimator structure is shown in Fig. 2 where i_g, ε and k represent the input signal, the error signal and the damping factor, respectively. From Fig. 2, the closed-loop transfer functions of the general SOGI can be obtained as

$$G(s) = \frac{i_{ac}(s)}{i_g(s)} = \frac{k\omega_0 s}{s^2 + k\omega_0 s + \omega_0^2} \quad (2)$$

Let's assume the output grid current signal $i_g(t)$, comprises of both ac and dc components. Then the grid current can be described as:

$$i_g(t) = i_{dc} + i_{ac} = A_0 + A_1 sin(\omega_s t + \varphi_s) \quad (1)$$

Where i_{dc} and i_{ac} are the dc and ac component in the grid current, respectively, and A_0, is the amplitude of dc component. Beside A_1, ω_s and φ_s are the amplitude, frequency, and phase-angle of ac components, respectively. In s-domain, $i_g(s)$ can be expressed by (4)

$$i_g(s) = \frac{A_0}{s} + \frac{A_1(\omega_s cos\varphi_s + s\, sin\varphi_s)}{s^2 + \omega_0^2} \quad (4)$$

Therefore, $i_{ac}(s)$ can be derived from (2) and (4)

$$i_{ac}(s) = \frac{k\omega_0 s}{s^2 + k\omega_0 s + \omega_0^2} * \left(\frac{A_0}{s} + \frac{A_1(\omega_s cos\varphi_s + s\, sin\varphi_s)}{s^2 + \omega_0^2} \right) \quad (5)$$

Applying the inverse Laplace transform to (5), the steady-state output of $i_{ac}(t)$ can be obtained as:

$$i_{ac}(t) = mA_1 sin(\omega_s t + \varphi_s + \varphi) \quad (6)$$

$$m = \frac{k\omega_0\omega_s}{\sqrt{k^2\omega_0^2\omega_s^2 + (\omega_0^2 - \omega_s^2)^2}} \quad (7)$$

$$\varphi = \arctan \frac{\omega_0^2 - \omega_s^2}{k\omega_0\omega_s} \quad (8)$$

Therefore, the dc component and harmonics can be determined by simply subtracting i_{ac}, from grid current. According to [26], the damping factor k in (2) can be simply determined by deciding an appropriate value for the settling time t_s. In which stability is guaranteed for all k > 0. The lower value of k, the better filtering effect of $G(s)$. But the stronger dependence on the resonant frequency ω_0 and a very low value of k degrades the dynamic performance of the SOGI. In this paper, based on the analysis of the SOGI's bode

plots, considering the tradeoff between the transient response speed and filtering performance, the parameter of *k* is chosen as *0.1*.

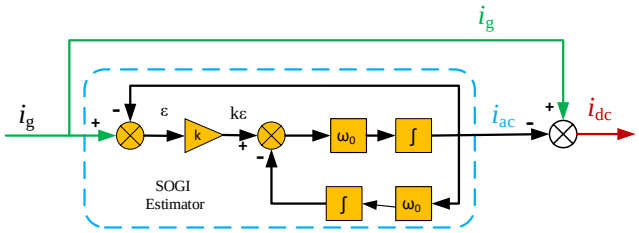

Fig-2: Block diagram structure for a dc current component extraction based on SOGI.

3.2 DC Component Suppression with PSO-FPID Controller

The block diagram of the proposed control scheme is shown in Fig. 3, which is composed of three parts: A Second-Order Generalized Integrator (SOGI), PSO-FOPID controller, and QPR controller. The SOGI will estimate dc components in the grid current, and the PSO-FOPID controller realizes zero steady-state error for the dc suppression loop. In this work, the QPR controller is adopted for the inner-loop current control which, has better steady-state performance and ensures the high-power quality of the system output current, compared with the conventional PI or PID controller.

Recently, PI and PID controllers have been widely used in most dc component compensation methods because of their simple structure and robust performance in a wide range of operating conditions. However, in addition to difficulty tuning the gains of PID controllers properly, the PID controller cannot provide a perfect control performance for the highly nonlinear and uncertain controlled plant. Therefore, it is highly desirable to increase the capabilities of the PID controller beyond integral application by combining the merits of fractional order calculation and optimization algorithm. Fractional order PID controller has two extra parameters corresponding to the integral and differential terms of Integer order PID controller, which handles the system dynamics and nonlinearities with robustness and increases the flexibility for better design of control system. Furthermore, we employed a Particle Swarm Optimization (PSO) algorithm-based FOPID controller, which has the advantages of strong adaptation, self-learning capability and online parameter regulation capability combined with FOPID controller for minimization of dc component injection into the grid.

The PSO algorithm adjusts the control parameters *(k_p,k_i,k_d, λ and μ)* of the $PI^{\lambda}D^{\mu}$ controller by tracking dc component error at the sampling time point and eliminating these errors in a very short finite time. As mentioned earlier, the PSO algorithm is aimed to achieve a minimum dc current error in the next sampling period.

For this purpose, it is necessary to first get the dc current error. The error is defined as the absolute difference between the reference dc current and the obtained dc component extracted from the grid current. Then, a cost function F(s) is applied to the obtained dc current error. The cost function is defined in equation (21). Because the PSO method is an excellent optimization methodology and promising approach for obtaining optimal FOPID controller parameters problem; therefore, this study develops the PSO-FOPID to search optimal FOPID parameters. And this controller is called the PSO-fractional order PID controller, which we applied for dc current suppression.

3.3 Particle Swarm Optimization Algorithm

PSO is one of the most powerful optimization algorithm methods, especially for achieving the best solutions for nonlinear systems. This technique is an evolutionary algorithm that is based on the natural behaviors of schools of fishes and flocks of birds that move around in a group at a D-dimensional space [28]. Each member of the populations in PSO is one solution candidate in the domain of search space. In the PSO algorithm, members of the group can learn from the experiences of each other, which directs members toward the best solution in the search space. PSO algorithm principles mainly depend on two factors, velocity and position of each candidate in the search space. In PSO, each member uses its own past memory and the knowledge of neighbors to find the best solution (*pbest*). *pbest* is the best solution of a particle amongst its own past iterations, as expressed by its highest fitness value. Amongst all individual *pbest* values the best fitness value is called the global best (*gbest*). *gbest* is considered as a solution candidate, it also guides the other particle member to move toward its neighbor's best global solutions in the next iterations, and thus, can cause the particles to trap in the local optimums. In the PSO algorithm at the beginning, it initializes the swarm by assigning a random value in the problem search space for each candidate solution. The position of the i^{th} particle is given by $\boldsymbol{X_i= X_{i1}, X_{i2},..., X_{id}}$ and its velocity is given by $\boldsymbol{V_i=[V_{i1}, V_{i2},..., V_{id}]}$. The optimal position of each particle is given by $\boldsymbol{P_i= P_{i1}, P_{i2},..., P_{id}}$ and the best global position is given by $\boldsymbol{[P_g= P_{g1}, P_{g2},..., P_{gd}]}$.

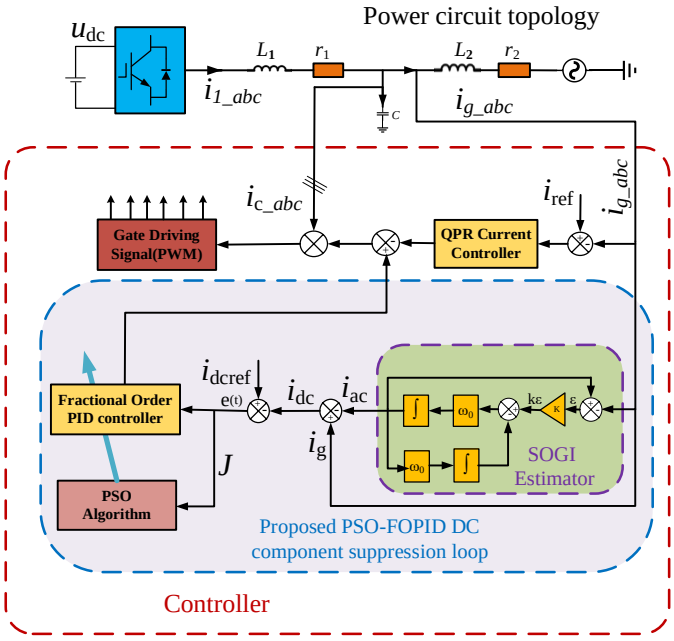

Fig-3:The block diagram of the proposed PSO-PI controller for three-phase inverter dc component suppression.

The value of the velocity of each member is updated by using equations (9) in every search iteration according to its own *pbest* and *gbest.*

$$V_i = \omega V_{i-1} + c_1 r_1 (pbest_i - x_i) + c_2 r_2 (gbest - x_i) \quad (9)$$

where (i = 1,2, ..., m), n is the iteration number, r_1, r_2 are random numbers between (0, 1). c_1 and c_2 , are the social rate and the cognitive rate, respectively. ω is the inertia weight, V_i and V_{i-1} denote the velocities of the new and old particles, respectively. The position is updated by

$$X_i = X_{i-1} + V_i \quad (10)$$

With more iteration, the best solution can be obtained as

$$x_i = \begin{cases} x_i, & if\ f(x_i) \le f(x_{i-1}) < 0 \\ x_{i-1}, & otherwise \end{cases} \quad (11)$$

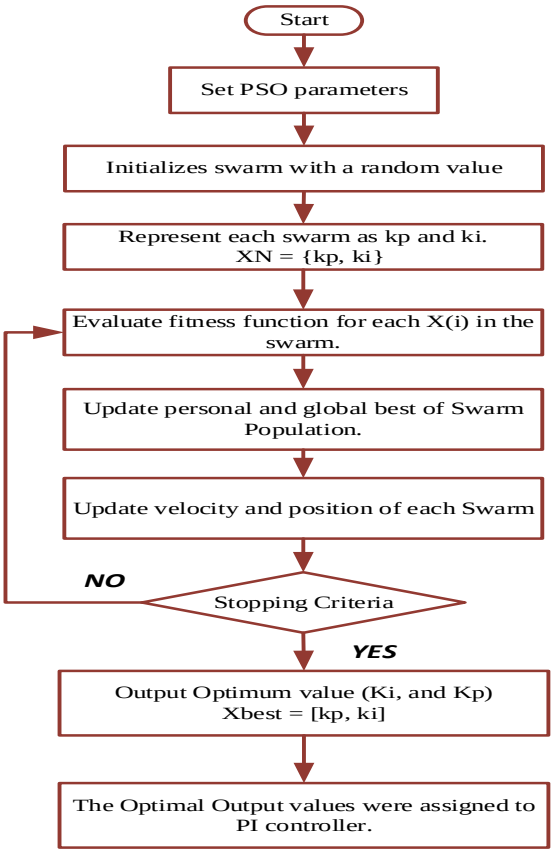

Fig-4:Flowchart of the PSO algorithm for the dc component suppression loop controller.

4. FRACTIONAL-ORDER PID CONTROLLER

4.1 Basic of Fractional-Order Calculus

There are many definitions of FOC; the three widely used definitions of Fractional-order calculus are, Riemann-Liouville, Grunwald-Letnikov, and Caputo approach [22-25]. Grunwald-Letnikov's definition is presented as follows:

$$ {}_aD_t^{\alpha} f(t) = \lim_{h \to 0} \frac{1}{h^{\alpha}} \sum_{r=0}^{\left[\frac{t-a}{h}\right]} (-1)^r \binom{n}{r} f(t - rh) \quad (12)$$

where h stands for the time step, $n-1 < a < n$, $[(t-a)/h]$, is integer part, and α, t are upper and lower limits of the operator, respectively. The binomial coefficient is evaluated by gamma function as in equation (x)

$$\binom{n}{r} = \frac{\Gamma(n+1)}{\Gamma(r+1)\Gamma(n-r+1)}, \quad (13)$$

The Riemann Liouville (RL) definition avoids using limit and sum, instead uses integer-order derivative and integral, which is presented as follows:

$$ {}_aD_t^{\alpha} f(t) = \frac{1}{\Gamma(n-\alpha)} \left(\frac{d}{dt}\right)^n \int_a^t \frac{f(\tau)}{(t-\tau)^{\alpha-n+1}} d\tau \quad (14) $$

$\Gamma(.)$, is a well-known gamma function defined as

$$ \Gamma(x) = \int_0^{\infty} t^{x-1} e^{-t} dt \quad (15) $$

The third commonly used definition of fractional order derivative is proposed by M.Caputo and defined by the following equation:

$$ D^{\alpha}|_a^t = {}_aD_t^{\alpha} f(t) = \frac{1}{\Gamma(n-\alpha)} \int_a^t \frac{f^{(n)}(\tau)}{(t-\tau)^{\alpha-n+1}} d\tau \quad (16) $$

With the development of FOC applications in the controller, new areas of control theory are appeared, namely fractional theory and fractional controller. Fractional order control theory is built up based on fractional calculus theory. Recent research studies have shown that Fractional-order controllers could perform better than integer-order controllers in terms of system performance and robustness.

4.2 Fractional Order PID Control

The fractional-order calculus (FOC) is one of the popular and newly emerging mathematics branches, which provides an efficient tool for many real situations related to infinite memory, fractional dimensions, and chaotic behavior.

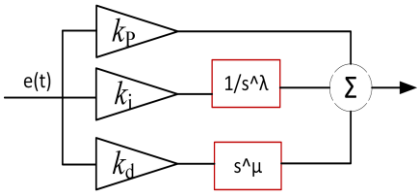

Fig-5: Block Diagram of PI^λ D^μ Controller.

The fractional-order differentiator can be described as a continuous differential-integrator operator, which is given by (9)

$$ dD_t^{\gamma} = \begin{cases} \frac{d^{\gamma}}{dt^{\gamma}}, & \Re(\gamma) > 0 \\ 1, & \Re(\gamma) = 0 \\ \int_a^t (d\tau)^{-\gamma}, & \Re(\gamma) < 0 \end{cases} \quad (17) $$

where, γ is the order of the differentiation and a is constant related to initial condition. Laplace transform is the most commonly used tool to describe a fractional-order system, which transforms from the time domain to the frequency domain. n^{th} order ($n \epsilon R$) derivative of a signal $x(t)$ at $t = 0$ is given by (x):

$$ L\{D^n x(t)\} = s^n X(s) \quad (18) $$

Let assume $a_i, b_i \epsilon R, \alpha, \beta \epsilon R^+$ and $\forall i \epsilon N^*$, the fractional calculus equation can be obtained as follows:

$$ (a_n D^{\alpha_n} + a_{n-1} D^{\alpha_{n-1}} + \cdots + a_0) y(t) = (b_m D^{\beta_m} + b_{m-1} D^{\beta_{m-1}} + \cdots + b_0) u(t) \quad (19) $$

Then by assuming initial conditions are zero, the transfer function of the fractional equation can be obtained as

$$ G(s) = \frac{U(s)}{Y(s)} = \frac{b_m D^{\beta_m} + b_{m-1} D^{\beta_{m-1}} + \cdots + b_0}{a_n D^{\alpha_n} + a_{n-1} D^{\alpha_{n-1}} + \cdots + a_0} \quad (20) $$

In this paper, a Fractional order PID control system is proposed and integrated into the DC suppression loop. The proposed fractional-order $PI^{\lambda}D^{\mu}$ controller, for dc current suppression loop, is shown in Fig. 6, where, $e(t)$ is the error signal, $G_S(s)$ is the transfer function of SOGI, $G_p(s)$ is the transfer function of $PI^{\lambda}D^{\mu}$ controller.

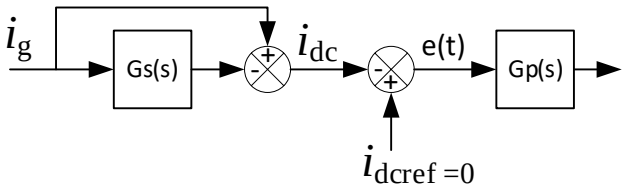

Fig-6: Block Diagram of simplified dc current suppression loop.

The transfer function of a conventional PID controller is shown in equation (xx) with three parameters.

$$ G_{PID}(s) = K_p + K_i \frac{1}{s} + K_d s \quad (21) $$

The Fractional-order PID controller introduces two more adjustable parameters λ and μ than the conventional PID controller, as shown in fig.2. The differential equation of the Fractional-order $PI^{\lambda}D^{\mu}$ the controller is given as the following:

$$ u(t) = K_p e(t) + K_i D_t^{-\lambda} e(t) + K_d D_t^{\mu} e(t) \quad (22) $$

The transfer function is given as:

$$ G_{FOPID}(s) = K_p + K_i \frac{1}{s^{\lambda}} + K_d s^{\mu} \quad (23) $$

Where K_p , K_i , and K_d , are the proportional, integral, and derivative gain, respectively. At the same time, λ and μ are

the two non-integer orders of the integral and derivative constants, respectively.

4.3 Parameter Tuning of Fractional Order PID Controller

The tuning process of the FOPID controller is done using the particle swarm optimization (PSO) method. The block diagram in Fig. 7 represents the use of the PSO algorithm to design the proposed fractional-order $PI^{\lambda}D^{\mu}$ Controller. J represents an objective function to be minimized for dc current suppression loop controller to find the optimum fractional-order $PI^{\lambda}D^{\mu}$, controller's parameters giving satisfactory responses. J is formulated as an integral of time multiplied absolute error (ITAE) between reference and dc component extracted from grid current.

$$\text{ITAE} = \int_0^{t_{max}} t|e(t)|dt \qquad (24)$$

Where $|e(t)|$ is the absolute value of the error (the error between reference and dc component extracted from grid current), t is a time, and t_{max}, is the maximum time.

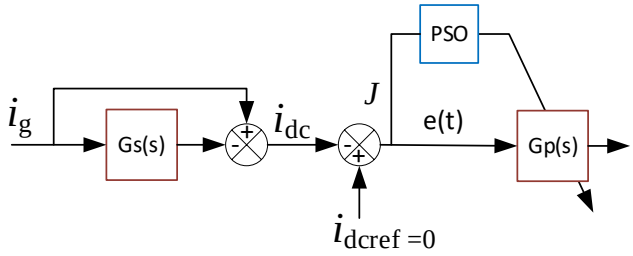

Fig-7: PSO-based fractional PID controller design

5. EXPERIMENTAL RESULTS

The proposed PSO-FOPID methods have been verified through simulation and Experiments. The simulation model is set up in the MATLAB/Simulink environment, and experimental verification is performed using a Hardware-In-Loop (HIL) test that could offer the most complex model-based design for interacting with the real-time platform. RT-LAB (OP4050) was used as the Real-Time Simulator for power stage emulation. Fig.8 shows the experimental setup, and the parameter specifications are given in Table I and Table II.

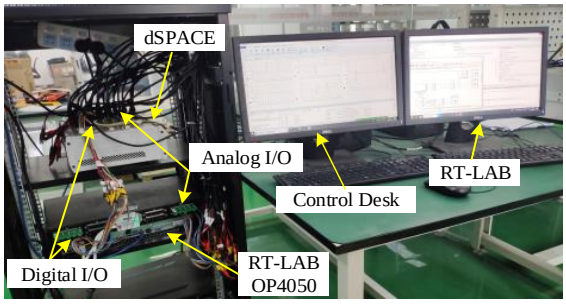

Fig-8: Configuration of the HIL experimental platform.

Table-1: PARAMETER SPECIFICATIONS OF THREE-PHASE LCL-GCCS

Symbol	PARAMETER	Values
V_{in}	Input voltage	700 V
V_g	Grid voltage	500 V_{dc}
f_o	Fundamental frequency	220 V
R_1	Fundamental frequency of the grid	50 Hz
R_2	Parasitic resistance of L_1	1 mF
L_1	Parasitic resistance of L_2	1 mH
L_2	Inverter inductance	2 mH
C_f	Filter capacitance	2.2 μF
L_2	Grid-side inductance	25 kHz

Table 2: PARAMETER SPECIFICATIONS OF PSO ALGORITHM

Symbol	PARAMETER	Values
n	Number of populations	50
I_{max}	Maximum No of Iteration	100
C_1	Weight coefficient 1	2
C_2	Weight coefficient 2	2
ω	Inertia Constant	1

To demonstrate how our proposed method suppresses dc components, dc-components of 3A in phase-A, -1.5A in phase-B, and -1.5A in phase-C are injected into the reference current. At the time point t= 0.2s, the dc suppression loop of the PSO-FOPID controller starts to operate. From Fig. 9-b, it is clear that the proposed method has a smooth and steady-state sinusoidal grid current waveform after one cycle. This shows the output DC component of current is almost reduced to zero, which fully demonstrates the effectiveness of the proposed method.

Fig. 10 and Fig. 11 shows DC current generated due to disparities of Power Transistors and DC current generated due to the unbalanced grid voltage. Fig. 10 (c) and Fig. 11 (c) The waveform of grid current with the proposed method. FFT analysis result of the grid-connected current is shown in

Fig.12, which shows the THD of the grid-current is only 4.00% that meets the harmonic requirement of grid-connected inverters (THD<5%).

The comparison results of the proposed second-order generalized integrator (SOGI), and sliding window double integral method (SWDIM) of dc current detection is shown in Fig. 13. At 0.2s, a dc current of step signal of 3A in phase A is added in reference current. The SWDIM methods take about 0.035s to estimate the dc current, while the proposed SOGI methods take only 0.025s, which shows the advantage of the quick dynamic response of the proposed method.

Fig. 14 shows the results of the comparative simulation analysis of the DC compensation scheme of the proposed method with the virtual capacitor concept and BP-PID approach. As shown in Fig.10(a), at the time point t= 0.2s, the dc component of 3A is injected into phase-A. It can be seen that with the virtual capacitor concept [12] and the BP-PID method [19], the DC component in the grid current is suppressed below 0.5 % of the rated current at t= 0.286s and t= 0.33s, respectively. However, with the proposed method, the DC component in the grid current is suppressed to less than 0.5% of the rated current at t= 0.243s (which only required 0.043s). Moreover, the overshoot for DC component suppression with the proposed method is much smaller than the virtual capacitor and BP-PID method. The

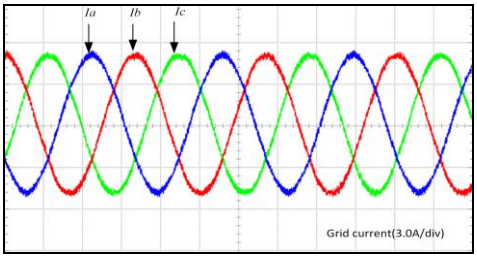

(a)

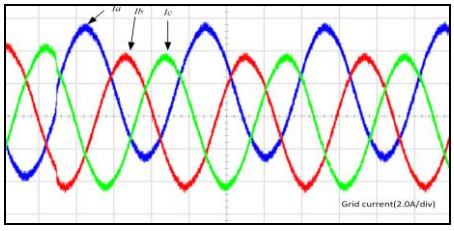

(b)

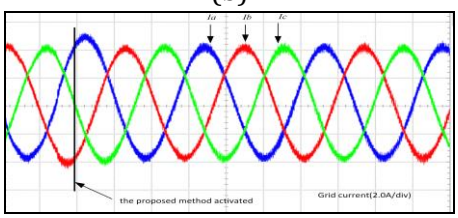

(c)

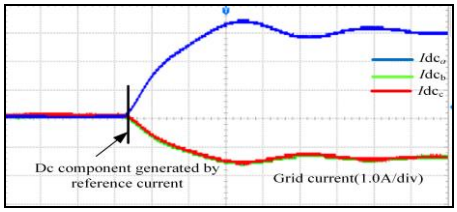

(d)

Fig-9: The waveform of grid current with and without the proposed method. (a) The steady-state waveform of grid current under original QPR control strategy. (b) The waveform of grid current without the proposed method. (c) The waveform of grid current with the proposed method. (d) dc component extracted from grid current.

Case I: DC Current Due to Disparities of Power Transistors

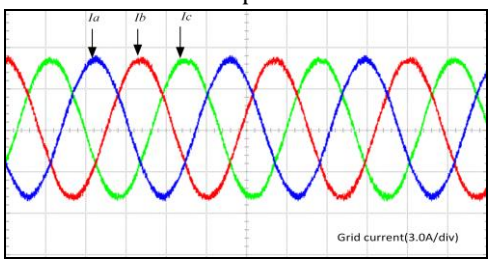

(a)

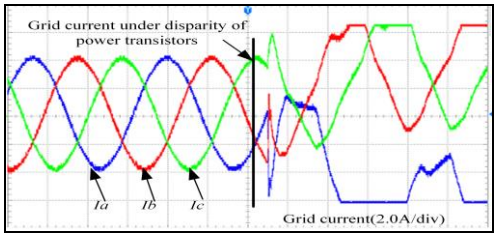

(b)

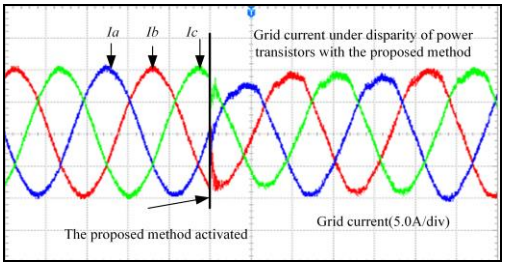

(c)

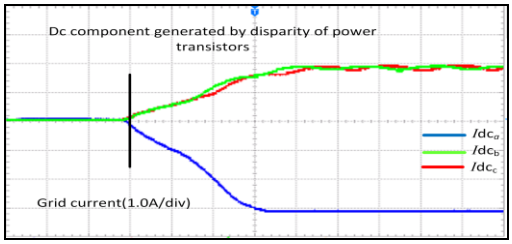

(d)

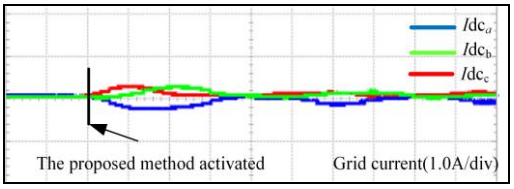

(e)

Fig-10: DC current generated due to disparities of Power Transistors. (a) The steady-state waveform of grid current under original QPR control strategy. (b) The waveform of grid current without the proposed method. (c) The waveform of grid current with the proposed method.

Case II:DC current due to the unbalanced grid voltage:

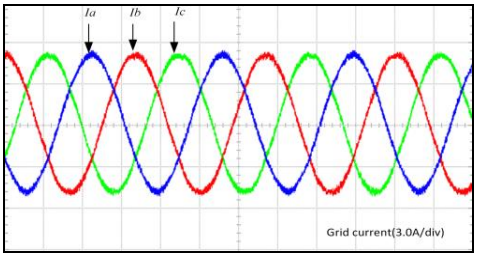

(a)

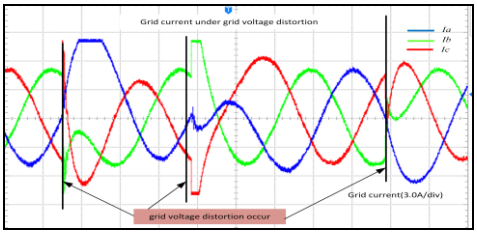

(b)

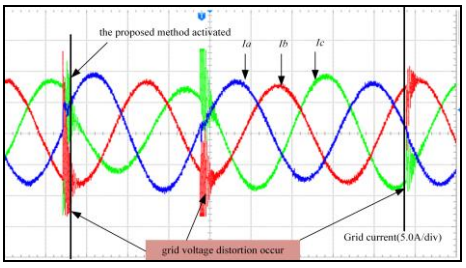

(c)

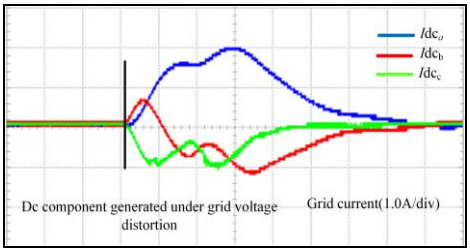

(d)

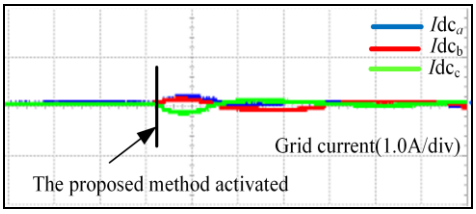

(e)

Fig-11: DC current generated due to grid voltage distortion. (a) The steady-state waveform of grid current under original QPR control strategy. (b) The waveform of grid current without the proposed method. (c) The waveform of grid current with the proposed method.

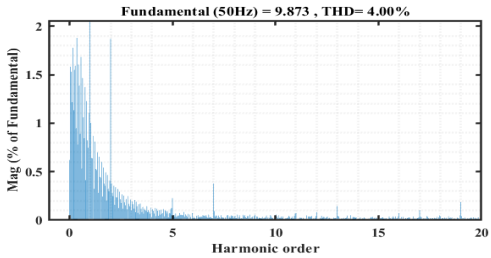

Fig-12: THD and harmonic spectrum of the inverter output current with the Proposed Method.

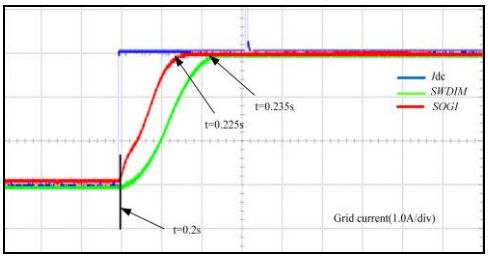

Fig-13: Comparison of dc component detection methods.

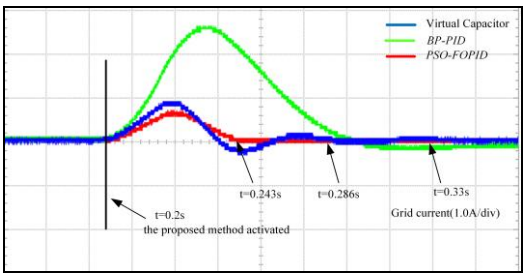

Fig-14: Comparison of DC component suppression results under the condition of injecting 3A DC component into the power grid.

6 CONCLUSIONS

This paper presents an effective dc current compensation technique for a three-phase grid-connected transformerless inverter. The SOGIs were employed for dc component extraction from grid current and mitigated using dc current suppression loop. An optimization technique based on

natural behaviors of schools of fish (PSO algorithms) is proposed for tuning parameters of FOPID controllers, which has the advantage of robustness, and global convergence capability to achieve fast and high accuracy parameter estimation. The objective function was chosen as the absolute error between the actual and estimated values, which is minimized by searching for the optimal value using the PSO algorithm. The proposed dc suppression technique enables robust suppression of dc injection into the utility grid under a wide range of dc uncertainties. The feasibility and effectiveness of the proposed scheme has been confirmed through simulation and experimental tests.

REFERENCES

[1] H. Xiao, "Overview of Transformerless Photovoltaic Grid-Connected Inverters," in IEEE Transactions on Power Electronics, vol. 36, no. 1, pp. 533-548, Jan. 2021, doi: 10.1109/TPEL.2020.3003721.

[2] M. N. H. Khan, M. Forouzesh, Y. P. Siwakoti, L. Li, T. Kerekes and F. Blaabjerg, "Transformerless Inverter Topologies for Single-Phase Photovoltaic Systems: A Comparative Review," in IEEE Journal of Emerging and Selected Topics in Power Electronics, vol. 8, no. 1, pp. 805-835, March 2020, doi: 10.1109/JESTPE.2019.2908672.

[3] B. Long, M. Zhang, Y. Liao, L. Huang and K. T. Chong, "An Overview of DC Component Generation, Detection and Suppression for Grid-Connected Converter Systems," in IEEE Access, vol. 7, pp. 110426-110438, 2019, doi: 10.1109/ACCESS.2019.2934175.

[4] "IEEE Recommended Practice for Utility Interface of Photovoltaic (PV) Systems," in IEEE Std 929-2000 , vol., no., pp.i-, 2000, doi: 10.1109/IEEESTD.2000.91304.

[5] W. M. Blewitt, D. J. Atkinson, J. Kelly, and R. A. Lakin, "Approach to low-cost prevention of DC injection in transformerless grid connected inverters," *IET Power Electron.*, vol. 3, no. 1, pp. 111–119, Jan. 2010.

[6] R. Gonzalez, J. Lopez, P. Sanchis and L. Marroyo, "Transformerless Inverter for Single-Phase Photovoltaic Systems," in IEEE Transactions on Power Electronics, vol. 22, no. 2, pp. 693-697, March 2007, doi: 10.1109/TPEL.2007.892120.

[7] T. Shimizu, O. Hashimoto and G. Kimura, "A novel high-performance utility-interactive photovoltaic inverter system," in IEEE Transactions on Power Electronics, vol. 18, no. 2, pp. 704-711, March 2003, doi: 10.1109/TPEL.2003.809375.

[8] R. Sharma, "Removal of DC offset current from transformerless PV inverters connected to utility," presented at the 40th International Universities Power Engineering Conference, Cork, Ireland, 2005, technique for transformerless, grid connected, H-bridge inverter systems," IEEE Trans. Power Electron., vol. 21, no. 5, pp. 1385–1393.

[9] M. Chen, D. Xu, T. Zhang, K. Shi, G. He and K. Rajashekara, "A Novel DC Current Injection Suppression Method for Three-Phase Grid-Connected Inverter Without the Isolation Transformer," in IEEE Transactions on Industrial Electronics, vol. 65, no. 11, pp. 8656-8666, Nov. 2018, doi: 10.1109/TIE.2018.2808916.

[10] L. Bowtell and A. Ahfock, "Direct current offset controller for transformerless single-phase photovoltaic grid-connected inverters," *IET Renewable Power Generation,* vol. 4, no. 5, pp. 428-437, 2010, doi: 10.1049/iet-rpg.2009.0043.

[11] M. Armstrong, D. J. Atkinson, C. M. Johnson, and T. D. Abeyasekera, "Auto-Calibrating DC Link Current Sensing Technique for Transformerless, Grid Connected, H-Bridge Inverter Systems," *IEEE Transactions on Power Electronics,* vol. 21, no. 5, pp. 1385-1393, 2006.

[12] B. Long *et al.*, "Design and implementation of a virtual capacitor based DC current suppression method for grid-connected inverters," *ISA Transactions,* vol. 92, pp. 257-272, 2019.

[13] Q. N. Trinh, P. Wang, Y. Tang and F. H. Choo, "Mitigation of DC and Harmonic Currents Generated by Voltage Measurement Errors and Grid Voltage Distortions in Transformerless Grid-Connected Inverters," in IEEE Transactions on Energy Conversion, vol. 33, no. 2, pp. 801-813, June 2018, doi: 10.1109/TEC.2017.2763240.

[14] M. Armstrong, D. J. Atkinson, C. M. Johnson, and T. D. Abeyasekera, "Auto-Calibrating DC Link Current Sensing Technique for Transformerless, Grid Connected, H-Bridge Inverter Systems," *IEEE Transactions on Power Electronics,* vol. 21, no. 5, pp. 1385-1393, 2006.

[15] C. Lu, B. Zhou, J. Lei and J. Shan, "Mains Current Distortion Suppression for Third-Harmonic Injection Two-Stage Matrix Converter," in IEEE Transactions on Power Electronics, vol. 36, no. 6, pp. 7202-7211, June 2021, doi: 10.1109/TPEL.2020.3039596.

[16] B. Guo et al., "Cost-Effective DC Current Suppression for Single-Phase Grid-Connected PV Inverter," in IEEE Journal of Emerging and Selected Topics in Power Electronics, vol. 9, no. 2, pp. 1808-1823, April 2021, doi: 10.1109/JESTPE.2020.3029393.

[17] T. Mannen, I. Fukasawa and H. Fujita, "A New Control Method of Suppressing DC Capacitor Voltage Ripples Caused by Third-Order Harmonic Compensation in Three-Phase Active Power Filters," in IEEE Transactions on Industry Applications, vol. 54, no. 6, pp. 6149-6158, Nov.-Dec. 2018, doi: 10.1109/TIA.2018.2849751.

[18] S. N. Vukosavić and L. S. Perić, "High-Precision Active Suppression of DC Bias in AC Grids by Grid-Connected Power Converters," in IEEE Transactions on Industrial Electronics, vol. 64, no. 1, pp. 857-865, Jan. 2017, doi: 10.1109/TIE.2016.2542126.

[19] L. Bo, L. Huang, Y. Dai, Y. Lu, and K. To Chong, "Mitigation of DC Components Using Adaptive BP-PID Control in Transformless Three-Phase Grid-Connected Inverters," Energies, vol. 11, no. 8, 2018.

[20] J. Jiang and X. Yuan, "Differential DC component suppression in three- phase non-isolated connected

inverter,'' *Power Capacitor Reactive Power Compensation*, vol. 39, no. 1, pp. 132–137, 2018.

[21] J. Z. Shi, "A Fractional Order General Type-2 Fuzzy PID Controller Design Algorithm," in IEEE Access, vol. 8, pp. 52151-52172, 2020, doi: 10.1109/ACCESS.2020.2980686.

[22] F. Meng, S. Liu, A. Pang and K. Liu, "Fractional Order PID Parameter Tuning for Solar Collector System Based on Frequency Domain Analysis," in IEEE Access, vol. 8, pp. 148980-148988, 2020, doi: 10.1109/ACCESS.2020.3016063.

[23] B. Hekimoğlu, "Optimal Tuning of Fractional Order PID Controller for DC Motor Speed Control via Chaotic Atom Search Optimization Algorithm," in IEEE Access, vol. 7, pp. 38100-38114, 2019, doi: 10.1109/ACCESS.2019.2905961..

[24] S. Seo and H. H. Choi, "Digital Implementation of Fractional Order PID-Type Controller for Boost DC–DC Converter," in IEEE Access, vol. 7, pp. 142652-142662, 2019, doi: 10.1109/ACCESS.2019.2945065.

[25] F. Meng, S. Liu and K. Liu, "Design of an Optimal Fractional Order PID for Constant Tension Control System," in IEEE Access, vol. 8, pp. 58933-58939, 2020, doi: 10.1109/ACCESS.2020.2983059.

[26] A. K. Mishra, S. R. Das, P. K. Ray, R. K. Mallick, A. Mohanty and D. K. Mishra, "PSO-GWO Optimized Fractional Order PID Based Hybrid Shunt Active Power Filter for Power Quality Improvements," in IEEE Access, vol. 8, pp. 74497-74512, 2020, doi: 10.1109/ACCESS.2020.2988611.

[27] M. A. Akhtar and S. Saha, "An Adaptive Frequency-Fixed Second-Order Generalized Integrator-Quadrature Signal Generator Using Fractional-Order Conformal Mapping Based Approach," in IEEE Transactions on Power Electronics, vol. 35, no. 6, pp. 5548-5552, June 2020, doi: 10.1109/TPEL.2019.2951427.

[28] L. Jia and X. Zhao, "An Improved Particle Swarm Optimization (PSO) Optimized Integral Separation PID and its Application on Central Position Control System," in IEEE Sensors Journal, vol. 19, no. 16, pp. 7064-7071, 15 Aug.15, 2019, doi: 10.1109/JSEN.2019.2912849.